J Appl Biomed
DOI: 10.32725/jab.2025.002
journal homepage: http://jab.zsf.jcu.cz

Journal of Applied Biomedicine

Original research article

Chemical composition and anticancer activity of *Psychotria montana* on MCF7 breast cancer cells: insights from *in vitro* (2D & 3D) studies and *in silico* analysis

Van Hung Hoang [1], Thi Kieu Oanh Nguyen [2], Phu Hung Nguyen [3] *, Thi Thanh Huong Le [4], Viet Hoang [4]

[1] *Thai Nguyen University, Tan Thinh Ward, Thai Nguyen City, Vietnam*
[2] *University of Science and Technology of Hanoi, Vietnam Academy of Science and Technology, 18 Hoang Quoc Viet, Cau Giay, Ha Noi, Vietnam*
[3] *Center for Interdisciplinary Science and Education, Thai Nguyen University, Tan Thinh Ward, Thai Nguyen City, Vietnam*
[4] *Thai Nguyen University of Sciences, Tan Thinh Ward, Thai Nguyen City, Vietnam*

Abstract
Aim: This study aimed to investigate the phytochemical composition of *Psychotria montana* extract (PME) and evaluate its inhibitory effects on MCF7 breast cancer cells.
Methods: The chemical composition of PME was analyzed using UPLC-QToF-MS. The effects of PME on cell proliferation were evaluated using the MTT assay. Flow cytometry was used for cell cycle and apoptosis analysis. The effects of PME on the transcription of cell cycle control genes were assessed using real-time PCR.
Results: UPLC-QToF-MS analysis revealed major compounds of PME, including terpenoids and flavonoids, with the potential to inhibit proliferation, migration, and induce apoptosis in MCF7 cancer cells. PME effectively suppressed MCF7 cell proliferation under 2D culture, with a low IC_{50} value of 34.7 μg/ml. PME also hindered cell migration ($p < 0.01$) and reduced spheroid number ($p < 0.001$) and size ($p < 0.001$) in serum-free 3D culture. Apoptosis analysis via nuclear staining with DAPI and flow cytometry revealed an increase in the number of apoptotic cells after PME treatment ($p < 0.001$). Additionally, the PME induced cell cycle arrest at the G0/G1 phase ($p < 0.05$). PME altered the expression of cell cycle control genes (cyclins and CDKs) as well as cancer suppressor genes including p16, p27, and p53 at the transcriptional level (mRNA). The results of molecular docking suggest that the compounds present in PME exhibit a high binding affinity for CDK3, CDK4, CDK6, and CDK8 proteins, which are essential regulators of the cell cycle.
Conclusion: Psychotria montana has the potential to inhibit cancer cells by inducing apoptosis and halting the cell cycle of MCF7 breast cancer cells

Keywords: Apoptosis; Breast cancer cells; Cell cycle; Migration; Spheroid

Highlights:
- *Psychotria montana* extract shows high terpenoids and flavonoids.
- *Psychotria montana* extract inhibits cell proliferation and migration in MCF7 cancer cells.
- *Psychotria montana* extract inhibits 3D spheroid formation from MCF7 cancer cells.
- *Psychotria montana* extract increases apoptotic cells and induces cell cycle arrest in MCF7 cancer cells.

Introduction

Breast cancer is recognized as a cancer type that occurs mainly in women, and the incidence of new cases is steadily increasing worldwide (Siegel et al., 2022). Various anti-breast cancer drugs have been widely utilized. However, common challenges encountered in breast cancer treatment with chemotherapeutic agents include the occurrence of adverse effects, the development of drug resistance in cancer cells during therapy, and high treatment costs (Balkhi et al., 2020; Burguin et al., 2021). The utilization of anticancer drugs derived directly from plant sources has attracted attention in laboratories worldwide due to its benefits, such as reducing adverse effects and lowering treatment costs (Ali et al., 2023; Khan et al., 2019). Furthermore, the combination of traditional medicinal plant extracts with modern synthetic anticancer drugs has also shown promising results in enhancing treatment effectiveness (Aziz et al., 2021; Cheon, 2021). Consequently, extensive research on the anticancer effects of medicinal plants in various models, in-

* **Corresponding author:** Phu Hung Nguyen, Center for Interdisciplinary Science and Education, Thai Nguyen University, Tan Thinh Ward, Thai Nguyen City, Vietnam; e-mail: phuhungnguyen@tnu.edu.vn
http://doi.org/10.32725/jab.2025.002
Submitted: 2024-10-04 • Accepted: 2025-03-20 • Prepublished online: 2025-03-21
J Appl Biomed 23/1: 12–25 • EISSN 1214-0287 • ISSN 1214-021X

cluding *in silico*, *in vitro*, and *in vivo* models, is being carried out across different cancer cell types (Khan et al., 2019; Shrihastini et al., 2021).

Psychotria montana (PM) is a plant species belonging to the genus *Psychotria*, found in several countries in Southeast Asia, including Vietnam, Indonesia, Malaysia, Thailand, and the Philippines (Schoch et al., 2020). Other taxonomic designations for this plant species include *Eumachia montana* ((Blume) I.M. Turner (GBIF Secretariat, 2023) and *Chassalia montana* (Blume) Miq (Schoch et al., 2020)). The chemical composition of certain species of the *Psychotria* genus has been identified, including bioactive compounds such as psychotropic, indole, quinolone, phenols, and aliphatic compounds (Bhambhani et al., 2021). These compounds have shown inhibitory effects on bacteria, viruses, and parasites (Yang et al., 2016). Other noteworthy biological activities attributed to *Psychotria* species include analgesic, anti-inflammatory, antioxidant, free radical scavenging, and antidepressant effects (Bristy et al., 2020; Calixto et al., 2016; Orji et al., 2020). In traditional medicine, certain species belonging to the *Psychotria* genus are also used for the treatment of respiratory disorders, gastric inflammation, colitis, and specific gynecological conditions in females. Furthermore, some species of the *Psychotria* genus exhibit hallucinogenic properties used in religious ceremonies (Martins and Nunez, 2015; Mba et al., 2022). Additionally, inflammatory and enzyme inhibitory activities against α-glucosidase, α-amylase, and cholesterol esterase have been reported in certain species of this genus (Mba et al., 2022). Presently, the available data on the anticancer potential of *Psychotria* is rather limited. Therefore, the objective of our study was to determine the anticancer effects of an ethanol extract of PM on breast cancer cells. The metabolite profile of this extract was described for the first time by a metabolomics approach.

Materials and methods

Preparation of the PME

The sample of *Psychotria montana* (Blume) Miq. was collected at Tam Dao National Park, Vietnam (latitude of 36°39′12.94″N and a longitude of 105°31′6.49″E), and is stored at Thai Nguyen University, with voucher specimen TNU2023.07. Leaf samples of *Psychotria montana* (Blume) Miq. were thoroughly washed with water multiple times and dried in a drying cabinet at a temperature of 40–42 °C for 48 h. After drying, the leaf samples were ground into a fine powder. Ten grams of this powder was soaked in 20 ml of 90% ethanol (Fisher Chemical, France) and shaken at 200 rpm for 48 h. The residue was separated from the solution by filtration through Whatman filter paper. The remaining solution was collected and concentrated by complete evaporation. The concentrated extract was dissolved in dimethyl sulfoxide (Thermo Fisher, USA) to a concentration of 100 mg/ml, stored at –20 °C, and diluted before use.

Metabolite profiling and putative identification of major compounds in PME

The metabolite profiling and identification of major compounds in this PME were conducted using a hyphenated system, coupling ACQUITY UPLC I-Class Plus chromatography and a high-resolution Xevo G3 ESI/QTOF mass spectrometer (Waters Corporation, USA) (Hoang et al., 2024). Samples were prepared by dissolving 10 mg of the abovementioned dried extract in 1 ml of MeOH and then filtering through a 0.22 µm membrane. One microliter of this solution was injected into the system, starting with separation on an ACQUITY UPLC BEH C18 column (130Å, 1.7 µm, 2.1 mm × 100 mm) (Waters Corporation, USA). A mixture of solvent A (H_2O + 0.1% FA) and solvent B (ACN + 0.1% FA) was used as the mobile phase with a flow rate of 0.3 ml/min and gradient elution as follows: initial at 50% B, then increased to 55% B from 0.5 to 1.0 min, reached 60% B from 1.0 to 6.0 min, subsequently increased to 80% B from 6.0 to 13.0, increased to 90% B from 13.0 to 23.0, increased to 99% from 23.0 to 31.0, and finally increased to 50% at 32 min before column equilibration for 3 min.

The mass spectra were generated by electrospray ionization in both positive and negative modes with the following parameters: capillary voltage, 3.00 kV; sample cone, 100 V; source temperature, 150 °C; desolvation temperature, 600 °C; cone gas, 30 l/h; and desolvation gas, 1,000 l/h. Analyses were run in full scan mode from m/z 50 to 1100. To obtain the parent ions and fragmentations of each molecule, the low-energy mode was set at a 6 V cone voltage, while a range of voltages from 15 to 40 V was set in the high-energy mode.

The data were acquired with Masslynx 4.2 software (Waters Corporation, USA), which was imported into UNIFI software for processing. The annotation of peaks was based on their typical fragmentation patterns released by a QToF mass spectrometer in comparison to the Waters Traditional Medicine Library (consisting of 10,000 compounds) (Waters Corporation, US).

Cell culture and treatment with PME

MCF7 breast cancer cells were seeded in 12-well culture dishes at a density of 2,000 cells/well. RPMI 1640 medium supplemented with 10% fetal bovine serum (FBS) and 1% ampicillin/streptomycin/amphotericin B (Invitrogen-Thermo Fisher, USA) was used as the culture medium. The cells were cultured at 37 °C with 5% CO_2 and 95% humidity. The cells were treated with various concentrations of PME (0, 0.05, 0.1, 0.2, and 0.5 mg/ml), depending on the analysis. As a control, the PME was replaced with an equivalent amount of medium. After 48 h, changes in cell morphology were assessed through observation using a Nikon Ts2 inverted phase-contrast microscope (Nikon, Japan).

Measurement of cell proliferation by MTT assay

MTT assay was performed as previously described (Huong Le et al., 2023). The culture medium was removed, and 100 µl of fresh culture medium containing MTT (Thermo Fisher, USA) at a concentration of 0.5 mg/ml was added to each well. The culture plate was then incubated at 37 °C and 5% CO_2 for 4 h. Subsequently, the culture medium containing MTT was removed, 100 µl of dimethyl sulfoxide (VWR, France) was added to each well, and the plates were incubated at 37 °C for 15 min. Cell proliferation was indirectly determined by measuring the optical density at a wavelength of 570 nm using a multifunctional spectrophotometer (Multiskan Sky, Thermo Fisher, USA). The percentage of cell proliferation was calculated using the following formula:

$$\% \text{ Cell proliferation} = (\text{OD of the treated sample}/\text{OD of the control}) * 100$$

The experiments were independently repeated three times. The 50% inhibitory concentration (IC_{50}) for cell proliferation was calculated using GraphPad Prism software (version 5.0), according to the manufacturer's instructions.

3D spheroid culture

Tumorsphere (or spheroid) cultivation was carried out as detailed previously (Le et al., 2023a). MCF7 breast cancer cells

were cultured in DMEM/F12 culture medium without FBS on a nonadherent 24-well plate. The growth medium was amended with epithelial growth factor (EGF) and fibroblast growth factor (FGF) at a concentration of 20 ng/ml. The cell density employed for cultivation was 1,000 cells per well. The cells were subjected to PME treatment at concentrations of 50 and 100 µg/ml and incubated under conditions of 5% CO_2 at 37 °C. On day five of the culture, spheroid formation was analyzed utilizing the ImageJ software package.

Migration analysis

Migration analysis was performed as previously described, with a few minor modifications to suit the MCF7 cell line (Le et al., 2023a). MCF7 cells were cultured in a 96-well plate with RPMI 1640 medium and 10% FBS at 10,000 cells per well. After 48 h of culture, a separation strip was created using a pipette tip (200 microliters). Nonadherent cells were removed by washing twice with PBS. Fresh medium containing the PME at concentrations of 50 and 100 µg/ml was added to the culture wells. Control cells were cultured in medium without the PME. The narrowing of the boundary gap was measured after 24 h and 48 h using ImageJ software.

Morphological analysis of cell nuclei using DAPI staining

The assessment of nuclear morphological changes was carried out using the DAPI staining method under an inverted microscope, as previously described (Nguyen et al., 2025). MCF7 cells were cultured in a 24-well plate in RPMI 1640 medium. After 48 h of treatment with PME, the cells were fixed with 95% ethanol for 10 min. Subsequently, the cells were stained with 100 µl of DAPI solution (10 µg/ml) for 5 min. at 37 °C to visualize cell nuclei. Cell images were captured at 200× magnification using a Nikon T2U fluorescence microscope. The nuclear morphology characteristic of apoptosis was identified by features such as fragmentation, condensation, and a high fluorescence signal intensity when stained with DAPI, as compared to normal cells with large, uniform nuclei, and moderate fluorescence intensity.

Apoptosis and cell cycle analysis by flow cytometry

The analysis of apoptosis was performed using Annexin V apoptosis detection kit (Invitrogen Thermo Fisher, USA) as described in the manufacturer's instructions, with a few minor modifications to suit our laboratory conditions. The cells, numbering 20,000 in total, were cultured in a 24-well plate and fed RPMI 1640 medium for a period of 24 h. After this, the old medium was replaced with fresh medium containing PME at concentrations of 50 and 100 µg/ml, which the cells were exposed to for a period of 48 h. For cell cycle analysis, the cells were fixed in 70% ethanol and stained with PI for 30 min. Following this, the cells were harvested through trypsinization and centrifuged at a speed of 13,000 rpm for a period of 5 min. Subsequently, the cells were processed using the components of the kit according to the manufacturer's instructions. The flow cytometry analysis was conducted using a BD Accuri™ C6 Plus flow cytometer (BD Bioscience, USA), which analyzed the entire cell population. The experiments were repeated three times.

RNA extraction and analysing gene expression by real-time PCR

MCF7 breast cancer cells were seeded in 6-well plates at a density of 250,000 cells/well and then treated with medium containing PME at an IC_{50} concentration (34.7 µg/ml) for 24 h. Following this treatment, the culture medium was removed entirely and replaced with 1 ml of TRIzol (Invitrogen) to extract the total RNA. The cells were then centrifuged at 13,000 rpm for 5 mins to separate and recover the supernatant. Subsequently, 200 µl of chloroform was added to the recovered supernatant, followed by centrifugation and the addition of 500 µl of absolute ethanol. The RNA was then washed with 70% ethanol and centrifuged again. The RNA was dissolved in 80 µl of ion-free water, and its concentration was measured using a NanoDrop spectrophotometer at a wavelength of 260/280 nm.

Real-time polymerase chain reaction (PCR) analysis was carried out with the utilization of BIOFACT 2× Onestep master mix qRT-PCR, which incorporates SYBR Green I (BIOFACT, Korea), on the qTower3 system (Analytik Jena, Jena, Germany), adhering to the manufacturer's guidelines with an input RNA amount of 20 ng per reaction. The primer pairs applied for amplification are enumerated in Table 1. The PCR cycle comprises an initial denaturation phase at 95 °C for 15 min; 45 cycles of denaturation at 95 °C for 20 s, and annealing/extension at 60 °C for 20 s. The experiments were independently repeated three times. HPRT1 was employed as an internal control to determine the relative expression levels by the $2^{-\Delta\Delta Ct}$ method (Livak and Schmittgen, 2001).

Molecular docking

Preparation of protein structures: The 3D structures of CDK3, CDK4, CDK6, and CDK8 proteins were retrieved from the RCSB Protein Data Bank with IDs: 8H4R, S7J3, 5L2S, and 5HBJ (Suppl. Table S1 and Suppl. Fig. S1). The selected structures ensured the high-resolution criteria. Following the download of the PDB file, protein preparation for docking was carried out using the UCSF ChimeraX software to eliminate water molecules, small molecules, and non-protein ligands.

Preparation of ligand structures: All compounds (Table 2) were selected for molecular docking. Their 3D chemical structures were retrieved from the PubChem database and downloaded in the SDF format. Subsequently, OpenBabel v2.4.1 software was used to add charges and minimize energy, followed by saving the ligands in the PDBQT format.

Docking of ligands: Each ligand was docked with CDK3, CDK4, CDK6, and CDK8 proteins using PyRx 0.8 software with the AutoDock Vina method. Visual representations of binding interactions between CDK proteins and the 50 compounds were processed using BIOVIA Discovery Studio Visualizer v24.1.0.23298 software.

Data analysis

The collected data were analyzed using the specialized software GraphPad Prism 5.0. Statistical analysis was performed using one-way ANOVA, considering $p < 0.05$ to indicate statistical significance.

Results

Chemical profiling of PME

The dereplication of the PME was performed in a high-resolution mass spectrometry system (*UPLC-QToF-MS*) and then matched to the Waters Traditional Medicine Library using UNIFI software to annotate the metabolites. The exact mass and fragmentation pattern of the peaks in the high- and low-energy modes were used to identify the compounds in the abovementioned library. Fig. 1 shows the chromatograms acquired in negative and positive ionization modes. In terms of

Table 1. List of primers for real-time PCR

Gene name	Primer	Sequence (5' → 3')
CCND1	CCND1–Forward (F)	TCTACACCGACAACTCCATCCG
	CCND1–Reverse (R)	TCTGGCATTTTGGAGAGGAAGTG
CCND2	CCND2–F	TCTGGCATTTTGGAGAGGAAGTG
	CCND2–R	CTTCCAGTTGCGATCATCGACG
CCNB1	CCNB1–F	GACCTGTGTCAGGCTTTCTCTG
	CCNB1–R	GGTATTTTGGTCTGACTGCTTGC
CCNE1	CCNE1–F	TGTGTCCTGGATGTTGACTGCC
	CCNE1–R	CTCTATGTCGCACCACTGATACC
CDK2	CDK2–F	ATGGATGCCTCTGCTCTCACTG
	CDK2–R	CCCGATGAGAATGGCAGAAAGC
CDK3	CDK3–F	TCGCTGCTCAAGGAACTGAAGC
	CDK3–R	GTCCTGGCTGAGGAACTCAAAC
CDK4	CDK4–F	CCATCAGCACAGTTCGTGAGGT
	CDK4–R	TCAGTTCGGGATGTGGCACAGA
CDK6	CDK6–F	GGATAAAGTTCCAGAGCCTGGAG
	CDK6–R	GCGATGCACTACTCGGTGTGAA
CDK8	CDK8–F	GCTGATAGGAAGGTGTGGCTTC
	CDK8–R	CCGAGGTAACTGAACTGGCTTC
CDK9	CDK9–F	CCATTACAGCCTTGCGGGAGAT
	CDK9–R	CAGCAAGGTCATGCTCGCAGAA
P16	P16–F	CTCGTGCTGATGCTACTGAGGA
	P16–R	GGTCGGCGCAGTTGGGCTCC
P27	P27–F	CTCGTGCTGATGCTACTGAGGA
	P27–R	GGTCGGCGCAGTTGGGCTCC
P53	P53–F	CCTCAGCATCTTATCCGAGTGG
	P53–R	TGGATGGTGGTACAGTCAGAGC
HPRT1	HPRT1–F	CATTATGCTGAGGATTTGGAAAGG
	HPRT1–R	CTTGAGCACACAGAGGGCTACA

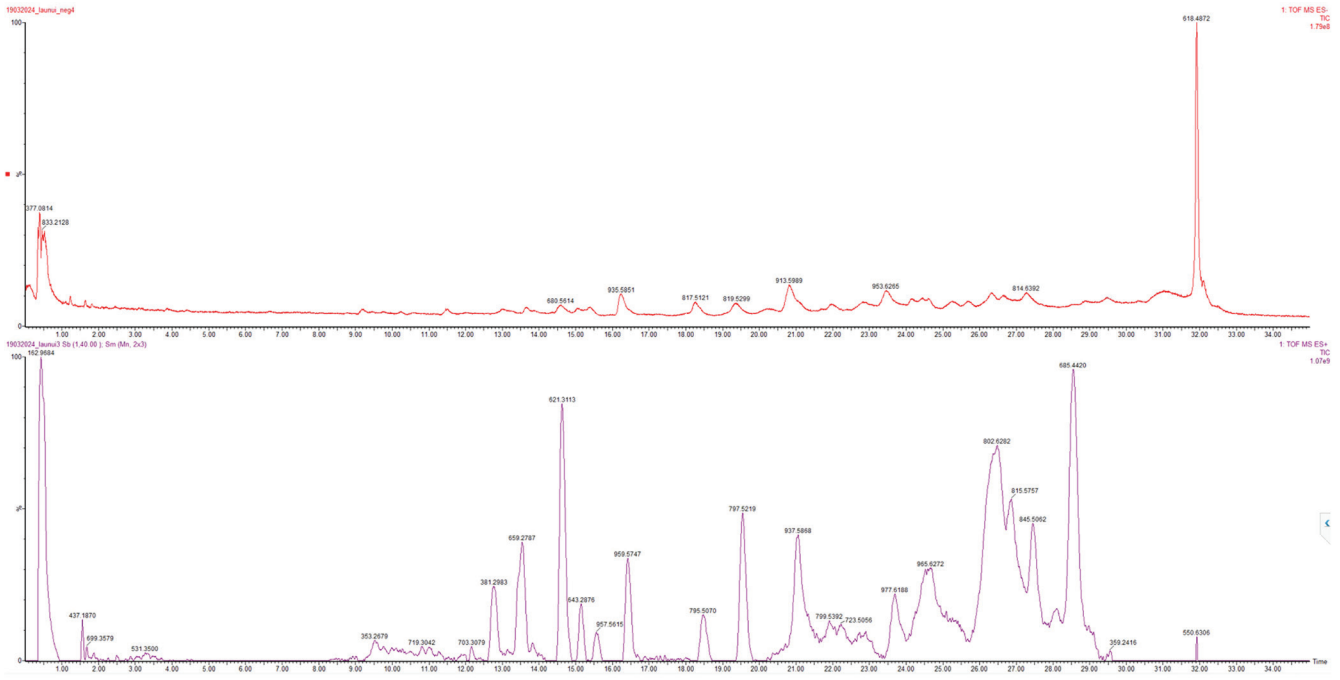

Fig. 1. TIC chromatograms of *P. montana* ethanolic extracts acquired using the UPLC-QToF-MS system with different electrospray ionization (ESI) modes. The red (upper) chromatogram represents peaks detected in negative ESI, while the violet (lower) represents those in positive ESI. The exact mass of MS spectrum at that RT was displayed on the peak of each chromatogram.

peak intensity, it is obvious that the positive mode facilitates ionization, so the number of peaks was much greater in the positive mode than in the negative mode. With respect to the data pre-processing parameters, we selected the peaks with a response of more than 15,000 counts to perform the annotation. The mass error threshold between the experimental and theoretical values was set to 5 ppm.

Table 2 shows the putative annotations of the peaks satisfying the optimized criteria. Overall, 50 compounds belonging to different classes, such as terpenoids, flavonoids, alkaloids, anthraquinones, coumarins, and saponins, were detected in the extract. Terpenoids form the major group dominating this profile, with 26 compounds. Next is the flavonoid group with 7 compounds. The minor classes include alkaloids, glycosides, saponins, and lignans, with 3–4 compounds for each group, but they may play an important role in the biological activity of PME. To the best of our knowledge, although there are many articles showing the chemical composition of the Rubiaceae family in general and the *Psychotria* genus in particular, no studies on this topic in *P. montana* exist. The number of compounds isolated from these species was also limited, and high variation in the profile was observed among genera and species within the Rubiaceae family (Martins and Nunez, 2015; Sumner et al., 2007). For the first time, the putative annotation profile of this species was described, which could provide a good source of information to explore in terms of chemotaxonomy and bioactivity.

Table 2. Metabolite profile of PME annotated putatively by matching with the Waters Traditional Medicine Library (Waters Corporation, US)

No	Annotation	Molecular formular	Observed RT (min)	Adducts	Observed m/z	Mass error (ppm)	Class
1	(+)-2-Northalrugosine	$C_{36}H_{38}N_2O_6$	4.57	[M+H]+	595.2789	–2.3	Alkaloids
2	1-Methyl-2-[(Z)-tetradec-8-enyl]quinolin-4-one	$C_{24}H_{35}NO$	31.7	[M+H]+	354.2798	1.9	Alkaloids
3	6,7-Dihydro-5',5'-dicapsaicin	$C_{36}H_{54}N_2O_6$	14.84	[M-H]–	609.3896	–2.2	Alkaloids
4	6'-O-Caffeoylerigeroside	$C_{20}H_{20}O_{11}$	1.56	[M+H]+	437.1077	–0.3	Phenolic acids
5	Pelargonidin	$C_{15}H_{11}ClO_5$	0.36	[M+H]+	272.0675	–1.5	Flavonoids
6	2''-O-Acetyl-3'-O-methylrutin	$C_{30}H_{34}O_{17}$	0.4	[M+H]+	667.1873	0.6	Flavonoids
7	Baohuoside II	$C_{26}H_{28}O_{10}$	0.51	[M+H]+	501.1759	0.7	Flavonoids
8	Andrographidine E	$C_{24}H_{26}O_{11}$	0.96	[M+H]+	491.1546	–0.4	Flavonoids
9	(2S,3S)-3,4',5,7-Tetrahydroxyflavanone	$C_{15}H_{12}O_6$	0.5	[M–H]–	287.0554	–2.6	Flavonoids
10	3',8-Diprenyl-4',5,7-trihydroxyflavone	$C_{25}H_{26}O_5$	3.89	[M–H]–	405.1715	2.0	Flavonoids
11	Tetramethoxyluteolin	$C_{19}H_{18}O_6$	0.39	[M–H]–, [M+HCOO]–	341.1045	4.2	Flavonoids
12	4'-O-beta-D-Glucosyl-5-O-methylvisamminol	$C_{22}H_{28}O_{10}$	1.24	[M–H]–	451.1605	–1.1	Coumarin
13	Gingerglycolipid A	$C_{33}H_{56}O_{14}$	3.2	[M+H]+, [M–H]–	677.3764, 675.3602	3.1	Fatty acid esters
14	Glyceryl linolenate II	$C_{39}H_{64}O_5$	19.57	[M+H]+	613.4816	–1.7	Fatty acid esters
15	1-O-Palmitoyl-2-O-Linolenoyl-3-O-(Beta-D-Galactopyranosyl)-L-Glycerol	$C_{43}H_{76}O_{10}$	29.28	[M+H]+	753.5493	–2.4	Fatty acid esters
16	Dichotomoside C	$C_{30}H_{40}O_{13}$	3.84	[M+H]+	609.256	2.9	Lignans
17	(+)-Pinoresinol-3,3-dimethylallyl ether	$C_{25}H_{30}O_6$	31.38	[M+H]+	427.2122	1.6	Lignans
18	1-[(4-Hydroxyphenyl)methyl]-4-methoxyphenanthrene-2,7-diol	$C_{22}H_{18}O_4$	33.68	[M+H]+	347.1285	2.1	Phenanthrols
19	Pseudoginsenoside Rt1 butyl ester	$C_{51}H_{82}O_{18}$	16.43	[M+H]+	983.5588	1.4	Saponins
20	Gypenoside LXVI	$C_{41}H_{70}O_{12}$	18.76	[M+H]+, [M–H]–	755.4957, 753.4818	2.3	Saponins
21	Ginsenoside Rh5	$C_{37}H_{64}O_9$	22.26	[M+H]+, [M–H]–	653.4612, 651.4469	–1.7	Saponins
22	Nuezhengalaside	$C_{18}H_{28}O_9$	0.46	[M+H]+, [M–H]–	389.1789, 387.1641	–4.5	Secoiridoid glucoside
23	(3beta)-Stigmast-5-en-3-yl 6-O-palmitoyl-beta-D-glucopyranoside	$C_{51}H_{90}O_7$	31.96	[M+H]+	815.6738	–2.6	Sterol glycoside
24	Sengosterone	$C_{29}H_{44}O_9$	2.49	[M+H]+	537.3059	0.2	Terpenoids
25	Uzarigenin	$C_{23}H_{34}O_4$	5.64	[M+H]+	375.2547	4.6	Steroid
26	12S-Hydroxyandrographolide	$C_{20}H_{32}O_6$	9.58	[M+H]+	369.2258	–3.7	Terpenoids
27	5α-Acetyl-1beta, 8-alpha-bis-cinnamoyl-4-alpha-hydroxydihydroagarofuran	$C_{35}H_{40}O_8$	14.63	[M+H]+	589.2815	3.3	Terpenoids

Table 2. ***(continued)***

No	Annotation	Molecular formular	Observed RT (min)	Adducts	Observed m/z	Mass error (ppm)	Class
28	3alpha-Hydroxy-6-oxo-5alpha-cholan-24-oic acid	$C_{24}H_{38}O_4$	15.06	[M+H]+	391.2851	2.0	Terpenoids
29	Andrographin F	$C_{25}H_{28}O_{13}$	24.45	[M+H]+	537.1626	4.4	Terpenoids
30	16beta-Hydroxyalisol B 23-acetate	$C_{32}H_{50}O_6$	26.81	[M+H]+	531.368	0.0	Terpenoids
31	Dihydro-beta-sitosteryl ferulate	$C_{39}H_{60}O_4$	28.05	[M+H]+, [M−H]−	593.4569, 591.4408	0.8	Terpenoids
32	Marianoside A	$C_{37}H_{62}O_8$	28.13	[M+H]+	635.449	−4.2	Terpenoids
33	3-O-(2,3-Dimethylbutanoyl)-13-O-dodecanoyl-20-acetylingenol	$C_{40}H_{62}O_9$	28.57	[M+H]+	687.4438	−4.1	Terpenoids
34	Triptocalline A	$C_{28}H_{42}O_4$	29.81	[M+H]+	443.3163	1.6	Terpenoids
35	Pterodondiol	$C_{15}H_{28}O_2$	22.88	[M−H]−	239.201	−2.9	Terpenoids
36	Eriojaposide B	$C_{25}H_{40}O_{11}$	10.61	[M−H]−	515.2475	−4.4	Terpenoids
37	Musennin	$C_{51}H_{82}O_{21}$	26.69	[M−H]−	1029.528	0.4	Triterpenoids
38	13-O-Acetylphorbol-20-linoleate	$C_{40}H_{60}O_8$	16.5	[M−H]−	667.4204	−1.7	Terpenoids
39	Gypenoside XLVII	$C_{53}H_{90}O_{22}$	16.25	[M−H]−	1077.582	−2.5	Terpenoids
40	3beta-Formyloxyresibufogenin	$C_{25}H_{32}O_5$	12.04	[M−H]−	411.2188	2.7	Terpenoids
41	Acacigenin B	$C_{40}H_{60}O_7$	31.88	[M−H]−	651.4287	3.1	Terpenoids
42	Arjunglucoside II	$C_{36}H_{58}O_{10}$	22.05	[M−H]−	649.3969	1.8	Terpenoids
43	5R,8R-Peroxydehydrotumulosic acid	$C_{31}H_{46}O_6$	14.39	[M−H]−	513.3207	−2.9	Terpenoids
44	Icariside B2	$C_{19}H_{30}O_8$	11.5	[M−H]−	385.1862	−1.6	Terpenoids
45	Gypenoside XLV	$C_{47}H_{80}O_{17}$	30.2	[M−H]−	915.5286	−4.0	Terpenoids
46	3-Hydroxytirucallic acid	$C_{30}H_{48}O_3$	6.1	[M−H]−	455.3543	2.7	Triterpenoids
47	Arvenin II	$C_{38}H_{58}O_{13}$	23.49	[M−H]−	721.384	4.9	Terpenoids
48	Lucialdehyde C	$C_{30}H_{46}O_3$	12.99	[M−H]−	453.3394	4.4	Triterpenoids
49	Ebelin lactone	$C_{30}H_{46}O_3$	13.64	[M−H]−	453.3397	5.0	Terpenoids
50	3,24-Dihydroxy-12-oleanen-22-one	$C_{30}H_{48}O_3$	14.16	[M−H]−	455.354	2.0	Terpenoids

PME inhibits cell proliferation in MCF7 breast cancer cells

The inhibitory effects on cell proliferation in response to various concentrations of PME are shown in Fig. 2A. At an initial concentration of 10 μg/ml of the PME, several gaps were observed on the surface of the cell culture dish. At concentrations ranging from 200 to 500 μg/ml, only a small proportion of living cells were observed, while most of the remaining cells exhibited a dying phenotype and lost their ability to adhere. The percent inhibition (Fig. 2B) ranged from 23.75 ± 5.96% at a concentration of 10 μg/ml PME ($p < 0.05$) to 82.1 ± 2.59% at a concentration of 500 μg/ml ($p < 0.001$). The IC50 value was 34.7 μg/ml (Fig. 2C). Thus, it can be concluded that the PME effectively suppressed the proliferation of MCF7 cells even at low concentrations.

PME inhibits the migration of MCF7 cells

Analysis of the impact of the PME on the migration of MCF7 cells was conducted after 24 and 48 h of treatment using PME at concentrations of 50 and 100 μg/ml (Fig. 3). The migratory ability of cells significantly differed between those treated with the PME and the control cells, with notable differences depending on the treatment concentration. After 24 h of incubation with PME, a significant difference in the extent of cell migration into the gap compared to that of the control cells ($p < 0.01$) was observed at both concentrations. Moreover, the width of the gap remained nearly unchanged compared to that in the initial state (at 0 h) when the cells were treated with 100 μg/ml PME. These observations suggest that cancer cells lose their proliferative and migratory abilities when treated with PME at high concentrations.

PME inhibits 3D spheroid formation in MCF7 cells

In current research on the cytotoxicity of potential anticancer candidates, the 3D spheroid analysis model is highly regarded because it has been demonstrated to closely resemble tumors in *in vivo* models compared to traditional 2D screening models (adherent cell culture) (Grigoreva et al., 2025). In this study, we analyzed the effect of PME on the formation of spheroids from MCF7 cells in serum-free medium and under nonadherent conditions.

The results (Fig. 4A) demonstrated that under untreated conditions, a substantial number of spheroids formed from individual cells. These spheroids exhibited large sizes and a bright color indicative of healthy cells. Conversely, cells treated with PME at a concentration of 50 μg/ml exhibited very few spheroids that were notably smaller in size than those of the control ($p < 0.001$). At higher concentrations (100 μg/ml), the extract suppressed the ability of MCF7 cells to form spheroids nearly completely. Compared with those of the untreated con-

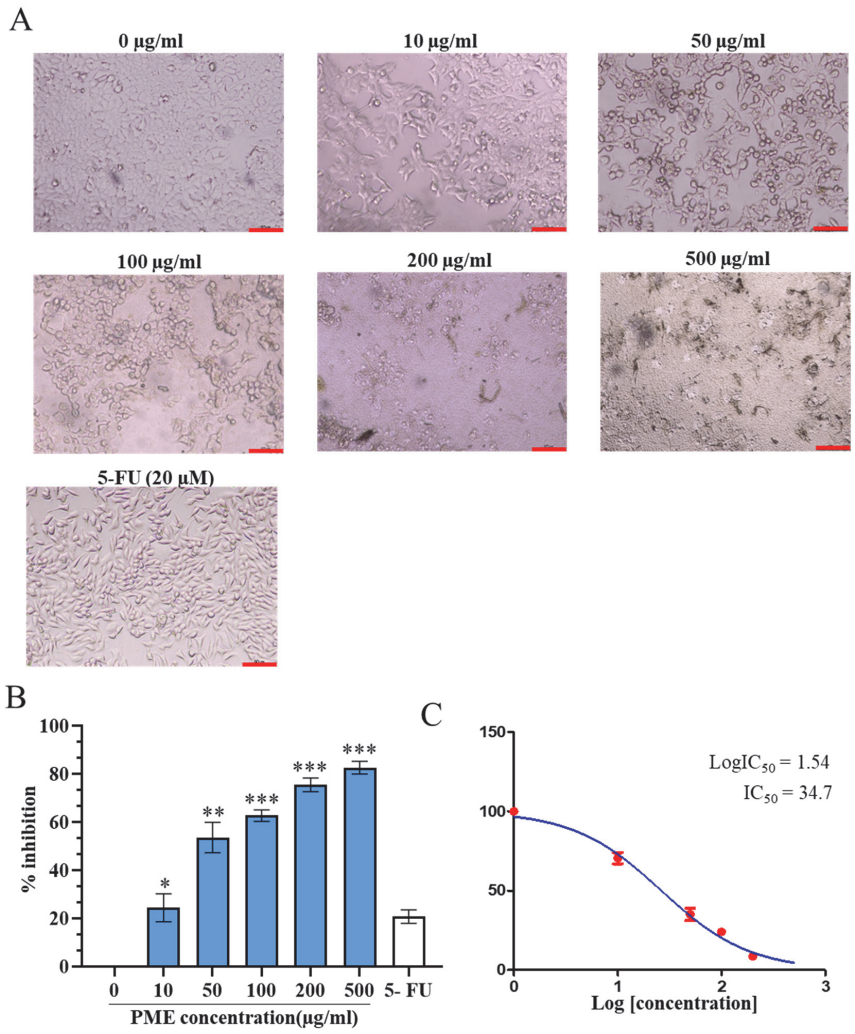

Fig. 2. Inhibitory effect of the PME on MCF7 cells. Cancer cells were treated with various concentrations of PME as indicated. (**A**) Cell morphology was assessed after 48 h of treatment using inverted microscopy. Scale bar = 90 µm. The percentage of inhibition, 5-Fluorouracil (5-FU) at 20 µM used as positive control (**B**). IC_{50} value (**C**) was determined using GraphPad 5.0. Mann–Whitney test, * $p < 0.05$, ** $p < 0.01$, *** $p < 0.001$ compared to control.

trol group, quantitative analyses revealed a significant reduction in both the number (Fig. 4B) and size (Fig. 4C) of spheroids formed ($p < 0.001$). Consequently, the extract effectively inhibited the formation of spheroids in serum-free culture conditions.

PME induces apoptosis in MCF7 cells

To assess the impact of PME on apoptosis in MCF7 cells, nuclear staining with DAPI was conducted using fluorescence microscopy, in addition to flow cytometry analysis with Annexin V staining. The images of nuclear staining with DAPI (Fig. 5A) indicated that only a few cells in the untreated control wells exhibited apoptotic features. The number of cells showing apoptotic nuclear characteristics (indicated by red arrows) was notably greater in cells treated with 50 µg/ml and 100 µg/ml PME. Flow cytometry analysis (Fig. 5B) demonstrated a marked increase in the percentage of apoptotic cells at concentrations of 50 µg/ml (21.1 ± 2.5%) and 100 µg/ml (39.4 ± 9.6%) compared to the control (1 ± 0.5%). These findings were in line with the results obtained from the DAPI nuclear staining analysis. Therefore, the PME triggered apoptosis in MCF7 cells.

The PME induces cell cycle arrest in MCF7 cells

The impact of PME on the cell cycle was assessed using flow cytometry (Fig. 6). The results indicated that PME induced cell cycle arrest at the G0/G1 phase. The proportion of cells in the G0/G1 phase in samples treated with the extract at concentrations of 50 µg/ml (66.3 ± 3.5%) and 100 µg/ml (68.7 ± 4.0%) significantly increased compared to that in the control (54.7 ± 2.5%). Moreover, the proportion of cells in the G2/M cell division phase significantly decreased compared to that in the control group. To assess changes in the transcription levels of key genes regulating the cell cycle and apoptosis, real-time PCR analysis was conducted. The results (Fig. 6C–E) indicated that out of the 14 genes related to cell cycle control, nine exhibited significant downregulation in expression, including CCNA2, CCNB1, CCND2, CCNE1, CDK3, CDK4, CDK6, CDK8, and CDK9. The reduction ranged from approximately 1.9-to 12.5-fold, notably with CCNB1 and CDK3 decreasing 12.5- and 9.6-fold, respectively. Other genes exhibiting notable decreases in expression were CCNA2 (1.9-fold), CCND2 (1.9-fold), CCNE1 (3.6-fold), CDK4 (7.3-fold), CDK6 (3-fold), CDK8 (2.7-fold), and CDK9 (1.9-fold). There were no significant changes observed in CCND1 expression compared to the control.

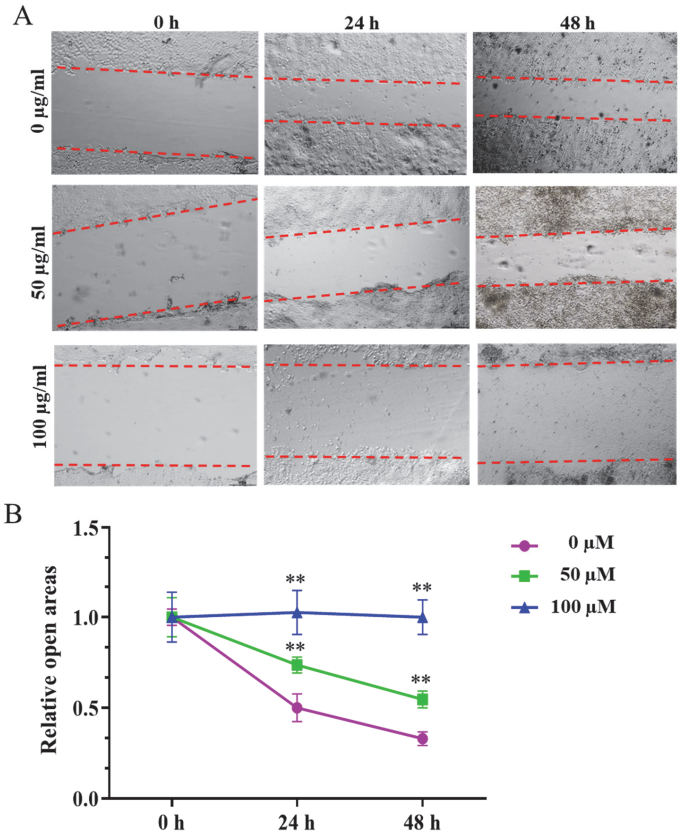

Fig. 3. Migration analysis shows the inhibitory effect of PME on cell migration in MCF7 cells. MCF7 cells were treated with PME at concentrations of 50 or 100 µg/ml for 24 h and 48 h. (**A**) Cell migration was observed at 24 and 48 h using inverted-microscopy Ts2, with a scale bar of 90 µm, and (**B**) quantitative analysis of relative open areas. ** $p < 0.01$, *** $p < 0.001$ compared to the control

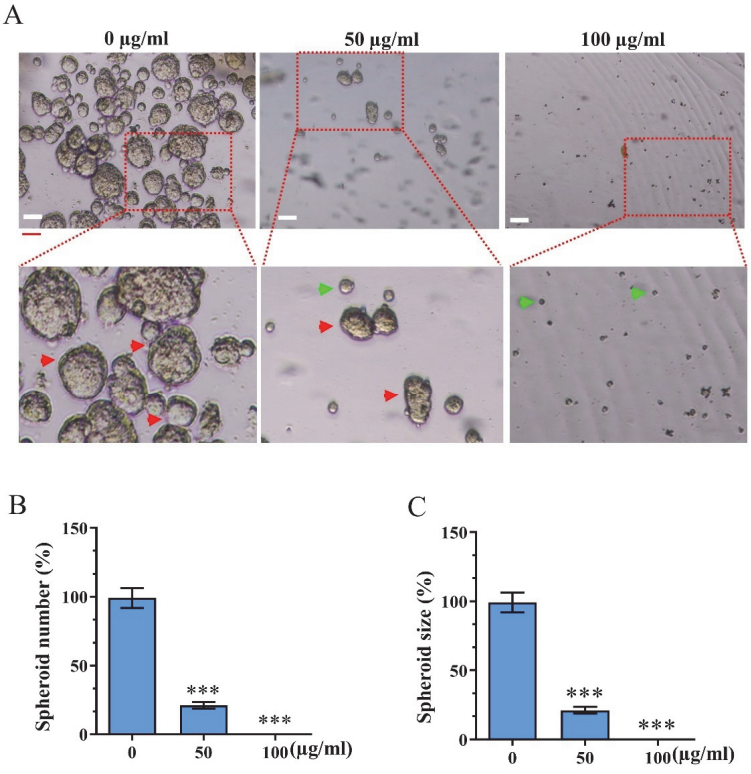

Fig. 4. The effect of PME on spheroid formation. MCF7 cells were treated with the extract at a concentration of 50 or 100 µg/ml. (**A**) Images of spheroids were captured under an inverted microscope at 100× magnification. The red arrow indicates spheroids, while the green arrow indicates single cells. Scale bar = 100 µm. The changes in spheroid number (**B**) and size (**C**) after 5 days of treatment are presented as the mean ± standard deviation ($n = 3$). Mann–Whitney test, *** $p < 0.001$ versus control.

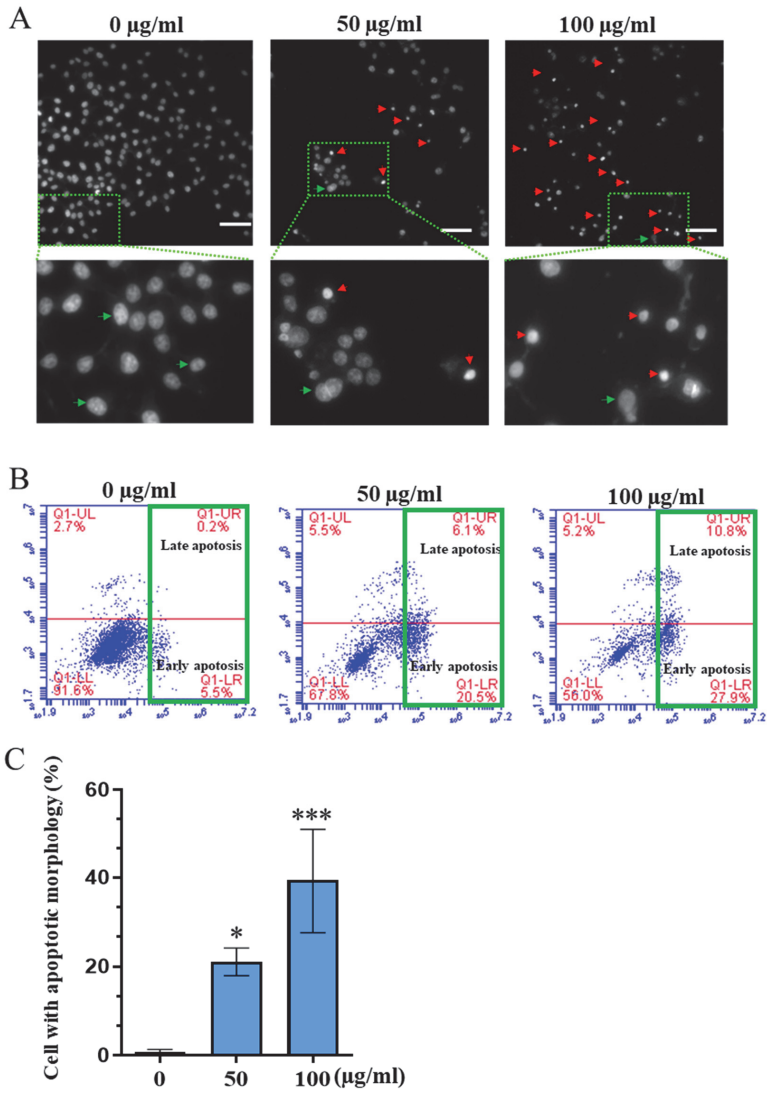

Fig. 5. Effect of PME on apoptosis. MCF7 cells were treated with the extract at concentrations of 50 or 100 µg/ml. (**A**) The nuclei were stained with DAPI and assessed under a fluorescence microscope (Nikon-T2U) at 100× magnification; scale bar = 100 µm. The green arrow indicates the nuclear morphology of normal cells, and the red arrow indicates that of apoptotic cells. (**B**) Dot plot images illustrating the apoptotic cell populations in the early and late stages as analyzed by flow cytometry. (**C**) The graph illustrating changes in the cell apoptosis ratio after 48 h of treatment is presented as the mean ± standard deviation (n = 3). Mann–Whitney test, * $p < 0.05$, *** $p < 0.001$ versus control.

In contrast to most cyclin and CDK genes, the group of genes concurrently controlling cell cycle and apoptosis (p16, p27, and p53) showed a significant increase in expression in response to PME, with p16, p27, and p53 levels rising by 2.9-fold, 1.8-fold, and 1.7-fold, respectively. Thus, it can be seen that PME intervened in the expression levels (mRNA) of key genes related to the cell cycle and apoptosis.

The interaction between compounds and CDK proteins

To predict candidate compounds with strong interactions with cell cycle regulatory proteins, molecular docking screening was conducted. The results (Fig. 7A) show that 50 compounds were identified, exhibiting varying degrees of interaction with the four target proteins: CDK3, CDK4, CDK6, and CDK8. The compound with the highest affinity for CDK3 was identified as compound 18 (–10.7 Kcal/mol); the compounds with the strongest affinities for CDK4, CDK6, and CDK8 were compound 10 (–11.1 Kcal/mol), compound 34 (–11.4 Kcal/mol), and compound 40 (–10.7 Kcal/mol), respectively (Table 3). The 2D and 3D spatial interactions between compounds 18, 10, 34, and 40 with CDK3, CDK4, CDK6, and CDK8 proteins are also illustrated (Fig. 7B–I).

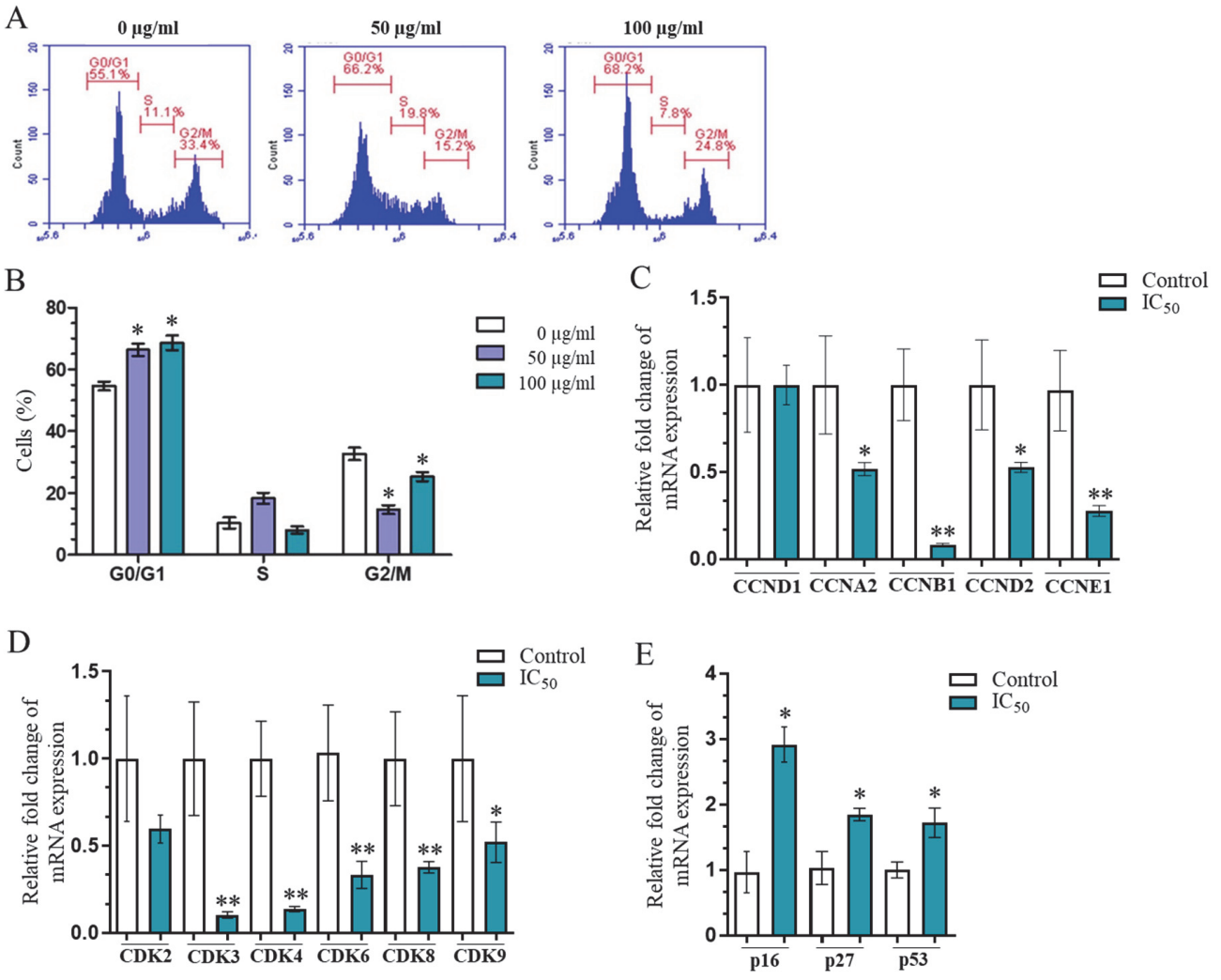

Fig. 6. Effects of PME on the cell cycle. (**A, B**) MCF7 cells were treated with PME at concentrations of 50 and 100 µg/ml, stained with PI, and analyzed using flow cytometry. * $p < 0.05$ versus control. (**C, D, E**) Effect of PME on the expression of genes regulating the cell cycle. Cells were treated with PME at IC50 concentration (34.7 µg/ml) for 24 h, and were then analyzed by Realtime PCR. Changes in mRNA levels of cyclin (**C**), CDK (**D**); and tumor suppressor (**E**) genes were analyzed by $2^{-\Delta\Delta Ct}$ method. Results are presented as mean ± SD ($n = 3$). Mann–Whitney test, * $p < 0.05$, ** $p < 0.01$.

Table 3. Docking scores and key interacting residues of selected compounds with target proteins

No	Ligand/compound	Protein	Score (Kcal/mol)	Hydrophilic	Hydrophobic	Electrostatic
10	3',8-Diprenyl-4',5,7-trihydroxyflavone	CDK4	–11.1	VAL96, HIS95, TYR17	ILE12, VAL20, ALA33, VAL72, PHE93, LEU147, ALA157	
18	1-[(4-Hydroxyphenyl)methyl]-4-methoxyphenanthrene-2,7-diol	CDK3	–10.7	LEU83, LYS89, ASP145, GLY13	ILE10, VAL18, ALA31, PHE80, SER84, LEU134	
34	Triptocalline A	CDK6	–11.4	VAL101		
40	3β-Formyloxyresibufogenin	CDK8	–10.7	ASP173, MET174, ARG356	VAL35, ALA50, ILE79, PHE97, ALA172	ASP103, ARG356

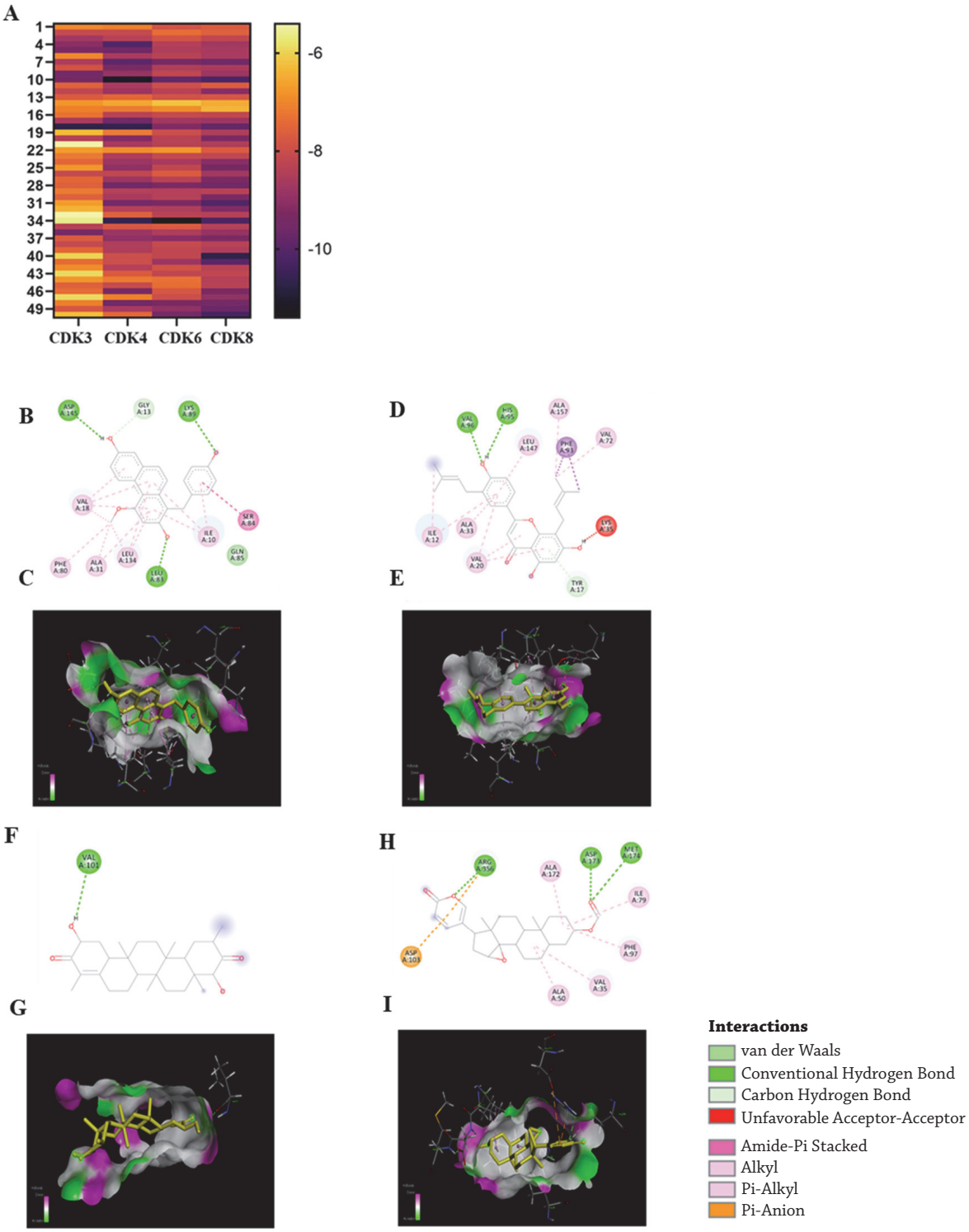

Fig. 7. Affinity of PME compounds with CDK proteins determined by molecular docking. (**A**) Docking scores are presented as a heatmap. (**B–I**) The 2D and 3D interaction models of high-affinity compounds with CDK3, CDK4, CDK6, and CDK8: (**B, C**) compound 18 with CDK3; (**D, E**) Compound 10 with CDK4; (**F, G**) compound 34 with CDK6; and (**H, I**) compound 40 with CDK8.

Discussion

The increasing global incidence of breast cancer poses a growing challenge for scientists in the search for effective drugs that can combat cancer cells without inducing drug resistance, while also being cost-effective and easy to produce with minimal side effects. As a result, there has been a shift toward exploring traditional and herbal medicines known for their historical efficacy against various diseases (Wang et al., 2023). In this study, the main constituents of the PME were characterized by liquid chromatography coupled to high-resolution mass spectrometry (UPLC-QtoF-MS). It should be noted that the level of metabolite identification is classified as putatively annotated compounds, which were identified without chemical reference standards and based on the similarity of MS spectra with libraries (Sumner et al., 2007). However, numerous parameters, such as retention time, MS fragmentation patterns, peak intensity, difference in exact mass, and typical fragment ions, were considered to ensure their annotation. Comprehensive metabolite profiling not only reveals the chemical composition of the PME, which is useful for chemotaxonomy but could also be useful for determining the bioactive compounds through different approaches, such as multivariate analysis, molecular networking, virtual screening, etc., in combination with bioactivity data (Yuliana et al., 2011). In this research, we examined the effect of *Psychotria montana*, a medicinal plant from Southeast Asia, on MCF7 breast cancer cells. The initial step in developing anticancer drugs typically involves screening for anti-proliferative effects and determining the IC_{50} value. Our study revealed that the PME hindered MCF7 cell proliferation *in vitro* with an IC_{50} value of 34.7 μg/ml, indicating its potent toxicity against these cells. Further analysis of the biological effects of the PME revealed a significant decrease in cell migration capacity compared to that of the control ($p < 0.01$). This finding suggested that PME has the potential to counteract the metastasis of MCF7 cancer cells. This is a crucial aspect in the development of herbal therapies for breast cancer, as demonstrated in various studies (Miyano et al., 2020; Zong et al., 2020). Several molecular mechanisms of migration, angiogenesis, and metastasis inhibition by herbal extracts and compounds have been reported, such as inhibition of the HIF-α signaling pathway (Zong et al., 2020), PI3K/Akt signaling pathway (Chen et al., 2022), MAPK pathway (ERK1/2) (Kang et al., 2012), regulation of the expression of angiogenesis and migration factors such as TGF-β1, MMP-9, and VEGF proteins (Mabasa et al., 2021), and suppression of epithelial-mesenchymal transformation (Zhang et al., 2021).

The use of 3D culture models in anticancer drug development has been widely discussed and studied and is considered advantageous compared to traditional adherent cell culture models. This approach enhances the similarity between *in vitro* (3D culture) and *in vivo* drug testing (Kapałczyńska et al., 2018). Tumor cells grown *in vitro* in spheroids or other 3D cultures exhibit tumor-like properties in terms of cell morphology, proliferation, polarity, and drug sensitivity. Recent reports have also indicated the ability of herbal extracts to inhibit spheroid formation and growth in various liver cancer cell lines (Huong Le et al., 2023), stomach cancer (Le et al., 2023b), and breast cancer (Nguyen-Thi et al., 2020). Our research data showed that PME significantly reduced both the number ($p < 0.001$) and size ($p < 0.001$) of MCF7 cell spheroids. This provides a crucial basis for conducting further investigations of the anticancer effect of PME, for example, using *in vivo* mouse xenograft models. Apoptosis induction has been acknowledged as a significant factor in weakening the proliferative capacity and metastasis of cancer cells (Hickman, 1992).

The induction of apoptosis is an essential approach in the development of contemporary cancer treatments (Carneiro and El-Deiry, 2020), and is a key focus of research on anticancer therapies in traditional Chinese medicine (An et al., 2019). In this study, we detected a significantly increased number of cells with condensed, shrunken, or fragmented DNA by DAPI staining, as well as apoptotic cells, as detected by Annexin V staining and flow cytometry, indicating a substantial increase in apoptosis in response to PME at a concentration of 50 μg/ml. Gene expression analysis using real-time PCR showed that PME regulated the simultaneous downregulation of key genes involved in cell cycle control. These changes are explained as the mechanisms leading to cell cycle arrest and apoptosis induction in MCF7 cells under the influence of PME. Previous reports have also discussed the apoptosis-inducing activity of some *Psychotria* species, such as *Psychotria ipecacuanha* on Jurkat T cells (Möller and Wink, 2007), and *Psychotria zombamonatana* and *Psychotria capensis* on THP-1 cells (Aro et al., 2019).

Among the 50 compounds identified by UPLC-QToF-MS, several compounds have been previously reported in studies for their characteristic biological activities, including inhibition of proliferation, induction of apoptosis, and cell cycle arrest. In a study on HT-29 colon cancer cells, Pelargonidin (compound 5) was demonstrated to induce apoptosis and arrest the cell cycle at the G2/M phase by regulating the activity of cell cycle-related genes such as CDC25C, CCNB1, CDK1, p53, and p21 (Karthi et al., 2016). Meanwhile, Andrographidine (compound 8) was shown to induce cell cycle arrest in MCF7 breast cancer cells (Banerjee et al., 2016). Previous studies also reported that Ginsenoside Rh5 (compound 21) inhibited the cell cycle at the G0/G1 phase in MCF7 cells by altering the transcription of genes such as CCND1, CCNE2, CDK4, p53, and others (Kim and Kim, 2015). Thus, it is evident that PME contains numerous compounds capable of inhibiting the cell cycle in MCF7 and other cancer cell lines. In this study, using molecular docking methods, the affinity of 50 compounds for 4 cyclin-dependent protein kinases (CDK3, CDK4, CDK6, and CDK8) was determined. The results indicate that the 4 compounds predicted to have the strongest binding with the CDKs are compound 10, 18, 34, and 40, respectively. The substances present in PME have not only demonstrated a considerable reduction in the expression levels of CDK proteins, but they may also inhibit these proteins by strongly binding to them, thus hindering the activity of the target proteins. Previously, using molecular docking methods, several natural compounds have also been identified as novel inhibitors of CDK4/CDK6 (Luo et al., 2022) or CDK8 (Aghahasani et al., 2024). CDK4 is also considered a target protein for inhibiting cancer cell growth by plant-derived compounds (Ashraf et al., 2022; Ji et al., 2023).

Conclusion

This finding suggests that PME has the potential to inhibit cell proliferation, induce apoptosis, and cause cell cycle arrest at the G0/G1 phase in MCF7 breast cancer cells. Additionally, compounds 10, 18, 34, and 40 are potential candidates with the ability to bind tightly to CDK proteins. Further investigations are warranted to elucidate the principal compounds responsible for this effect, thereby elucidating the mechanism by which *Psychotria montana* inhibits breast cancer cells.

Authorship contribution statement

Van Hung Hoang: Conceptualization, Writing – original draft, Funding acquisition, Writing – review and editing. *Phu Hung Nguyen:* Conceptualization, Methodology, Investigation, Data curation, Formal analysis, Visualization, Writing – original draft, Project administration, Resources. *Thi Kieu Oanh Nguyen, Thi Thanh Huong Le, Viet Hoang:* Methodology, Investigation, Data curation, Formal analysis, Writing – review and editing.

Ethical aspects and conflict of interest

The authors declare that they have no known competing financial interests or personal relationships that could have influenced the work reported in this paper.

References

Aghahasani R, Shiri F, Kamaladiny H, Haddadi F, Pirhadi S (2024). Hit discovery of potential CDK8 inhibitors and analysis of amino acid mutations for cancer therapy through computer-aided drug discovery. BMC Chem 18(1): 73. DOI: 10.1186/s13065-024-01175-6.

Ali M, Wani SUD, Salahuddin M, S N M, K M, Dey T, Zargar MI, Singh J (2023). Recent advance of herbal medicines in cancer – a molecular approach. Heliyon 9(2): e13684. DOI: 10.1016/j.heliyon.2023.e13684.

An W, Lai H, Zhang Y, Liu M, Lin X, Cao S (2019). Apoptotic Pathway as the Therapeutic Target for Anticancer Traditional Chinese Medicines. Front Pharmacol 10: 758. DOI: 10.3389/fphar.2019.00758.

Aro AO, Dzoyem JP, Goddard A, Fonteh P, Kayoka-Kabongo PN, McGaw LJ (2019). *In vitro* Antimycobacterial, Apoptosis-Inducing Potential, and Immunomodulatory Activity of Some Rubiaceae Species. Front Pharmacol 10: 185. DOI: 10.3389/fphar.2019.00185.

Ashraf MA, Sayed S, Bello M, Hussain N, Chando RK, Alam S, Hasan MdK (2022). CDK4 as a phytochemical based anticancer drug target. Inform Med Unlocked 28: 100826. DOI: 10.1016/j.imu.2021.100826.

Aziz B, Khurshid A, Mahmood R, Khan JA, Javaid S, Alam M, et al. (2021). Study of synergistic effects of *Ficus Carica* leaves extract mediated chemo-photodynamic therapy on rhabdomyosarcoma cells. Photodiagnosis Photodyn Ther 36: 102565. DOI: 10.1016/j.pdpdt.2021.102565.

Balkhi B, Alqahtani S, Altayyar W, Ghawaa Y, Alqahtani Z, Alsaleh K, Asiri Y (2020). Drug utilization and expenditure of anticancer drugs for breast cancer. Saudi Pharm J 28(6): 669–674. DOI: 10.1016/j.jsps.2020.04.007.

Banerjee M, Chattopadhyay S, Choudhuri T, Bera R, Kumar S, Chakraborty B, Mukherjee SK (2016). Cytotoxicity and cell cycle arrest induced by andrographolide lead to programmed cell death of MDA-MB-231 breast cancer cell line. J Biomed Sci 23: 40. DOI: 10.1186/s12929-016-0257-0.

Bhambhani S, Kondhare KR, Giri AP (2021). Diversity in Chemical Structures and Biological Properties of Plant Alkaloids. Molecules 26(11): 3374. DOI: 10.3390/molecules26113374.

Bristy TA, Barua N, Montakim Tareq A, Sakib SA, Etu ST, Chowdhury KH, et al. (2020). Deciphering the Pharmacological Properties of Methanol Extract of *Psychotria calocarpa* Leaves by *In Vivo, In Vitro* and *In Silico* Approaches. Pharmaceuticals 13(8): 183. DOI: 10.3390/ph13080183.

Burguin A, Diorio C, Durocher F (2021). Breast Cancer Treatments: Updates and New Challenges. J Pers Med 11(8): 808. DOI: 10.3390/jpm11080808.

Calixto NO, Pinto MEF, Ramalho SD, Burger MCM, Bobey AF, Young MCM, et al. (2016). The Genus *Psychotria*: Phytochemistry, Chemotaxonomy, Ethnopharmacology and Biological Properties. J Braz Chem Soc 27(8): 1355–1378. DOI: 10.5935/0103-5053.20160149.

Carneiro BA, El-Deiry WS (2020). Targeting apoptosis in cancer therapy. Nat Rev Clin Oncol 17(7): 395–417. DOI: 10.1038/s41571-020-0341-y.

Chen P, Wang B, Li M, Cui C, Liu F, Gao Y (2022). Celastrol inhibits the proliferation and migration of MCF-7 cells through the leptin-triggered PI3K/AKT pathway. Comput Struc Biotechnol 20: 3173–3181. DOI: 10.1016/j.csbj.2022.06.042.

Cheon C (2021). Synergistic effects of herbal medicines and anticancer drugs: A protocol for systematic review and meta-analysis. Medicine 100(46): e27918. DOI: 10.1097/MD.0000000000027918.

GBIF Secretariat (2023). GBIF Backbone Taxonomy. Checklist dataset DOI: 10.15468/39omei accessed via GBIF.org on 2025-03-17.

Grigoreva TA, Kindt DN, Sagaidak AV, Novikova DS, Tribulovich VG (2025). Cellular Systems for Colorectal Stem Cancer Cell Research. Cells 14(3): 170. DOI: 10.3390/cells14030170.

Hickman JA (1992). Apoptosis induced by anticancer drugs. Cancer Metastasis Rev 11(2): 121–139. DOI: 10.1007/BF00048059.

Hoang VH, Le TTH, Nguyen PH, Hoang V, Pham VK, Nguyen TKO, Can DQH (2024). Acorus gramineus extract decreases cancer stem cell properties and stimulates ROS signaling pathway in HepG2 hepatocellular carcinoma cells. Pharmacol Res – Mod Chin Med 13: 100548. DOI: 10.1016/j.prmcm.2024.100548.

Huong Le TT, Nguyen MQ, Nguyen VP, Hoang VH, Nguyen PH (2023). Methanol Extract of *Ficus pumila* L. Inhibits Proliferation, Induces Apoptosis and Arrests the Cell Cycle in HepG2 Live Cancer Cells. Asian J Plant Sci 22: 423–433. DOI: 10.3923/ajps.2023.423.433.

Ji J, Liu W, Xu Y, Xu Z, Lv M, Feng J, et al. (2023). WXJ-202, a novel Ribociclib derivative, exerts antitumor effects against breast cancer through CDK4/6. Front Pharmacol 13: 1072194. DOI: 10.3389/fphar.2022.1072194.

Kang YH, Yang IJ, Shin HM (2012). Herbal formula HMC05 prevents human aortic smooth muscle cell migration and proliferation by inhibiting the ERK1/2 MAPK signaling cascade. J Nat Med 66(1): 177–184. DOI: 10.1007/s11418-011-0573-3.

Kapałczyńska M, Kolenda T, Przybyła W, Zajączkowska M, Teresiak A, Filas V, et al. (2018). 2D and 3D cell cultures – a comparison of different types of cancer cell cultures. Arch Med Sci 14(4): 910–919. DOI: 10.5114/aoms.2016.63743.

Karthi N, Kalaiyarasu T, Kandakumar S, Mariyappan P, Manju V (2016). Pelargonidin induces apoptosis and cell cycle arrest via a mitochondria mediated intrinsic apoptotic pathway in HT29 cells. RSC Adv 6: 45064–45076. DOI: 10.1039/C5RA20984F.

Khan T, Ali M, Khan A, Nisar P, Jan SA, Afridi S, Shinwari ZK (2019). Anticancer Plants: A Review of the Active Phytochemicals, Applications in Animal Models, and Regulatory Aspects. Biomolecules 10(1): 47. DOI: 10.3390/biom10010047.

Kim SJ, Kim AK (2015). Anti-breast cancer activity of Fine Black ginseng (*Panax ginseng* Meyer) and ginsenoside Rg5. J Ginseng Res 39(2): 125–134. DOI: 10.1016/j.jgr.2014.09.003.

Le TTH, Ngo TH, Nguyen TH, Hoang VH, Nguyen VH, Nguyen PH (2023a). Anti-cancer activity of green synthesized silver nanoparticles using *Ardisia gigantifolia* leaf extract against gastric cancer cells. Biochem Biophys Res Commun 661: 99–107. DOI: 10.1016/j.bbrc.2023.04.037.

Le TTH, Nguyen PH, Nguyen VP, Nguyen TN (2023b). *Ardisia gigantifolia* ethanolic extract inhibits cell proliferation and targets cancer stem cells in gastric cancer. Asian Pac J Trop Biomed 13(6): 258–267. DOI: 10.4103/2221-1691.378600.

Livak KJ, Schmittgen TD (2001). Analysis of Relative Gene Expression Data Using Real-Time Quantitative PCR and the $2^{-\Delta\Delta CT}$ Method. Methods 25(4): 402–408. DOI: 10.1006/meth.2001.1262.

Luo L, Wang Q, Liao Y (2022). The Inhibitors of CDK4/6 from a Library of Marine Compound Database: A Pharmacophore, ADMET, Molecular Docking and Molecular Dynamics Study. Mar Drugs 20(25): 319. DOI: 10.3390/md20050319.

Mabasa R, Malemela K, Serala K, Kgakishe M, Matsebatlela T, Mokgotho M, Mbazima V (2021). Ricinus communis Butanol Fraction Inhibits MCF-7 Breast Cancer Cell Migration, Adhesion,

and Invasiveness. Integr Cancer Ther 20: 153473542097768. DOI: 10.1177/1534735420977684.

Martins D, Nunez C (2015). Secondary Metabolites from Rubiaceae Species. Molecules 20(7): 13422–13495. DOI: 10.3390/molecules200713422.

Mba JR, Zouheira D, Dairou H, Yadang FSA, Gael NN, Ayong L, et al. (2022). *In Vitro* Antioxidant, Anti-Inflammatory, and Digestive Enzymes Inhibition Activities of Hydro-Ethanolic Leaf and Bark Extracts of *Psychotria densinervia* (K. Krause) Verdc. Adv Pharmacol Pharm Sci 2022: 8459943. DOI: 10.1155/2022/8459943.

Miyano K, Eto M, Hitomi S, Matsumoto T, Hasegawa S, Hirano A, et al. (2020). The Japanese herbal medicine Hangeshashinto enhances oral keratinocyte migration to facilitate healing of chemotherapy-induced oral ulcerative mucositis. Sci Rep 10(1): 625. DOI: 10.1038/s41598-019-57192-2.

Möller M, Wink M (2007). Characteristics of Apoptosis Induction by the Alkaloid Emetine in Human Tumour Cell Lines. Planta Med 73(13): 1389–1396. DOI: 10.1055/s-2007-990229.

Nguyen PH, Le TTH, Can DQH, Le TNT, Hoang V, Ngo HP, et al. (2025). Anticancer potential of *Ampelopsis cantoniensis* extract: Inducing apoptosis, cell cycle arrest, and targeting cancer stem cells in HepG2 liver cancer cells. Biocatal Agric Biotechnol 64: 103521. DOI: 10.1016/j.bcab.2025.103521.

Nguyen-Thi LH, Nguyen ST, Tran TP, Phan-Lu CN, Van Pham P, The Van T (2020). Anti-cancer Effect of Xao Tam Phan *Paramignya trimera* Methanol Root Extract on Human Breast Cancer Cell Line MCF-7 in 3D Model. Adv Exp Med Biol 1292: 13–25. DOI: 10.1007/5584_2018_148.

Orji OU, Awoke JN, Harbor C, Igwenyi IO, Obasi OD, Ezeani NN, Aloke C (2020). Ethanol leaf extract of *Psychotria microphylla* rich in quercetin restores heavy metal induced redox imbalance in rats. Heliyon 6(9): e04999. DOI: 10.1016/j.heliyon.2020.e04999.

Schoch CL, Ciufo S, Domrachev M, Hotton CL, Kannan S, Khovanskaya R, et al. (2020). NCBI Taxonomy: a comprehensive update on curation, resources and tools. Database (Oxford) 2020: baaa062. DOI: 10.1093/database/baaa062.

Shrihastini V, Muthuramalingam P, Adarshan S, Sujitha M, Chen JT, Shin H, Ramesh M (2021). Plant Derived Bioactive Compounds, Their Anti-Cancer Effects and *In Silico* Approaches as an Alternative Target Treatment Strategy for Breast Cancer: An Updated Overview. Cancers (Basel) 13(24): 6222. DOI: 10.3390/cancers13246222.

Siegel RL, Miller KD, Fuchs HE, Jemal A (2022). Cancer statistics, 2022. CA Cancer J Clin 72(1): 7–33. DOI: 10.3322/caac.21708.

Sumner LW, Amberg A, Barrett D, Beale MH, Beger R, Daykin CA, et al. (2007). Proposed minimum reporting standards for chemical analysis: Chemical Analysis Working Group (CAWG) Metabolomics Standards Initiative (MSI). Metabolomics 3(3): 211–221. DOI: 10.1007/s11306-007-0082-2.

Wang H, Chen Y, Wang L, Liu Q, Yang S, Wang C (2023). Advancing herbal medicine: enhancing product quality and safety through robust quality control practices. Front Pharmacol 14: 1265178. DOI: 10.3389/fphar.2023.1265178.

Yang H, Zhang H, Yang C, Chen Y (2016). Chemical Constituents of Plants from the Genus *Psychotria*. Chem Biodivers 13(7): 807–820. DOI: 10.1002/cbdv.201500259.

Yuliana ND, Khatib A, Choi YH, Verpoorte R (2011). Metabolomics for bioactivity assessment of natural products. Phytother Res 25(2): 157–169. DOI: 10.1002/ptr.3258.

Zhang Z, Lin M, Wang J, Yang F, Yang P, Liu Y, et al. (2021). Calycosin inhibits breast cancer cell migration and invasion by suppressing EMT via BATF/TGF-β1. Aging (Albany NY) 13(12): 16009–16023. DOI: 10.18632/aging.203093.

Zong S, Tang Y, Li W, Han S, Shi Q, Ruan X, Hou F (2020). A Chinese Herbal Formula Suppresses Colorectal Cancer Migration and Vasculogenic Mimicry Through ROS/HIF-1α/MMP2 Pathway in Hypoxic Microenvironment. Front Pharmacol 11: 705. DOI: 10.3389/fphar.2020.00705.